Structure, Dynamics, and Ion Conductance of the Phospholamban Pentamer

Christopher Maffeo and Aleksei Aksimentiev*
Department of Physics, University of Illinois at Urbana-Champaign, Champaign, Illinois

ABSTRACT A 52-residue membrane protein, phospholamban (PLN) is an inhibitor of an adenosine-5′-triphosphate-driven calcium pump, the Ca^{2+}-ATPase. Although the inhibition of Ca^{2+}-ATPase involves PLN monomers, in a lipid bilayer membrane, PLN monomers form stable pentamers of unknown biological function. The recent NMR structure of a PLN pentamer depicts cytoplasmic helices extending normal to the bilayer in what is known as the bellflower conformation. The structure shows transmembrane helices forming a hydrophobic pore 4 Å in diameter, which is reminiscent of earlier reports of possible ion conductance through PLN pentamers. However, recent FRET measurements suggested an alternative structure for the PLN pentamer, known as the pinwheel model, which features a narrower transmembrane pore and cytoplasmic helices that lie against the bilayer. Here, we report on structural dynamics and conductance properties of the PLN pentamers from all-atom (AA) and coarse-grained (CG) molecular dynamics simulations. Our AA simulations of the bellflower model demonstrate that in a lipid bilayer membrane or a detergent micelle, the cytoplasmic helices undergo large structural fluctuations, whereas the transmembrane pore shrinks and becomes asymmetric. Similar asymmetry of the transmembrane region was observed in the AA simulations of the pinwheel model; the cytoplasmic helices remained in contact with the bilayer. Using the CG approach, structural dynamics of both models were investigated on a microsecond timescale. The cytoplasmic helices of the CG bellflower model were observed to fall against the bilayer, whereas in the CG pinwheel model the conformation of the cytoplasmic helices remained stable. Using steered molecular dynamics simulations, we investigated the feasibility of ion conductance through the pore of the bellflower model. The resulting approximate potentials of mean force indicate that the PLN pentamer is unlikely to function as an ion channel.

INTRODUCTION

Muscle cells respond to external nerve stimuli by releasing Ca^{2+} ions from a storage organelle called the sarcoplasmic reticulum (SR). The Ca^{2+} exposes myosin binding sites on actin filaments, which allows myosin to ratchet along actin and cause the muscle fibers to contract. For muscle fibers to relax, Ca^{2+} must be transported from the cytoplasm back to the SR. Sarco(endo)plasmic reticulum Ca^{2+}-ATPase (SERCA) resides in the membrane of the SR and transports two Ca^{2+} ions against a concentration gradient by using the energy of adenosine-5′-triphosphate hydrolysis. The uptake of Ca^{2+} by SERCA is regulated by the 52-residue membrane protein phospholamban (PLN), which acts as an inhibitor. The inhibition of SERCA by PLN is relieved upon phosphorylation of PLN at residue Ser^{16} by protein kinase A or at residue Thr^{17} by Ca^{2+}/calmodulin-dependent protein kinase (1). In the heart, inhibition of SERCA by PLN regulates muscle contraction, and mutations that alter PLN inhibitory function lead to degenerative cardiomyopathy (2). Because the PLN-SERCA complex regulates heart contraction, PLN is a target for the treatment of degenerative cardiac diseases and, hence, is of considerable interest to medicine (2).

Although >75% of PLN in a lipid bilayer membrane is pentameric (3), the only known function of PLN—SERCA inhibition—involves a PLN monomer and not a pentamer. One study reported Ca^{2+} ion conductance through PLN (4), suggesting that a PLN pentamer might form a Ca^{2+} ion channel. Another study found Cl^- ion conductance through an unidentified protein channel that could be blocked by the presence of a monoclonal anti-PLN antibody (5), suggesting that PLN could form a Cl^- ion channel. It has also been suggested that the PLN pentamer can store PLN monomers, thereby providing a mechanism for the cell to control inhibition of Ca^{2+}-ATPase (6).

Each protomer of the PLN pentamer consists of an amphipathic cytoplasmic helix (residues 1–16) and a hydrophobic transmembrane helix (residues 22–52) connected by an unstructured loop. It has been proposed that the flexibility of the cytoplasmic helix facilitates recognition of PLN by the regulators protein kinase A and Ca^{2+}/calmodulin-dependent protein kinase, and by Ca^{2+}-ATPase (7). The binding mechanism between SERCA and PLN is not fully understood, though mutagenesis studies indicate that some fragments of the cytoplasmic and upper transmembrane helices must unwind for binding to occur (8,9).

Several all-atom (AA) molecular dynamics (MD) studies (10–13) have been performed using a high-resolution NMR structure of the PLN monomer (Protein Data Bank access code 1N7L) (14). The studies revealed that the cytoplasmic helix of the PLN monomer is highly dynamic and can exhibit large collective motion. The studies also demonstrated that phosphorylation promotes unwinding of the C-terminus side of the cytoplasmic helix. The simulation results are in agreement with NMR measurements that indicate enhanced unwinding of the C-terminal end of the cytoplasmic helix

Submitted July 2, 2008, and accepted for publication March 20, 2009.

*Correspondence: aksiment@illinois.edu

Editor: David D. Thomas.

0006-3495/09/06/4853/13 $2.00

doi: 10.1016/j.bpj.2009.03.053

and faster, less restricted dynamics through the entire protein upon phosphorylation of Ser^{16} (15). Before publication of a high-resolution structure of the PLN pentamer, a computational model of its lower transmembrane region (residues 35–52) was constructed (Protein Data Bank access code 1PSL) (16) and used for an MD study of its ion conductance and wetting properties (17). The latter study indicated the possibility of water permeation through the pore of the pentamer and the favorable presence of K^+ over Cl^- ions.

The bellflower model (Protein Data Bank access code 1ZLL) (18) is a high-resolution NMR structure of the PLN pentamer that depicts a pore-forming coiled-coil structure with the transmembrane helix of the protomers strongly bent away from the pore near the cytoplasmic side. The cytoplasmic helices are oriented nearly normal to the bilayer, slightly inclined toward the center of the oligomer (see Fig. 1, *a* and *b*). The pinwheel model (Protein Data Bank access code 1XNU) (19) is a theoretical model based on Förster resonance energy transfer measurements that depicts transmembrane helices that are less bent and cytoplasmic helices that lie in the plane of the bilayer (see Fig. 6, *a* and *b*). Recent nuclear magnetic and electron paramagnetic resonance measurements show that the cytoplasmic helices of the PLN pentamer lie against the bilayer, favoring the pinwheel model over the bellflower model (20,21).

In this study, we use computational methods to investigate the conformational dynamics and ion conductance of the PLN pentamer. Through AA simulations, we evaluate the stability of the bellflower and pinwheel models in a lipid bilayer membrane. We use coarse-grained (CG) simulations to observe the formation of a micelle around the bellflower model, and AA simulations to study the dynamics of the bellflower in a micelle. We also use multiple CG simulations to determine structural fluctuations of the bellflower and pinwheel models on a microsecond timescale. Lastly, we examine the interaction of the pentamer's pore with water and ions to determine whether ion conduction is possible.

METHODS

MD methods

Except where specified, all MD simulations were performed using the program NAMD (22), the CHARMM27 force field (23) with the CMAP correction for backbone atoms (24), periodic boundary conditions, particle mesh Ewald full electrostatics computed over a 96 × 96 × 96 grid, and a smooth (10–12 Å) cutoff for van der Waals interactions. The temperature was held constant by applying Langevin forces (25) to all nonhydrogen atoms with a damping constant of 5 ps^{-1}. The NPT ensemble (constant number of particles (*N*), pressure (*P*), and temperature (*T*)) was maintained using Nosé-Hoover Langevin piston pressure control (26) at 1 atm. A 1-fs integration time step and multiple time-stepping (27) were used. All minimization was performed using the conjugate gradient method. Harmonic restraints, where applied, were imposed with a spring constant of 69.5 pN/Å. The TIP3P water model was used for all AA models (28). These systems were ionized by replacing water molecules at random positions with Cl^- or K^+ ions until the desired concentration was attained.

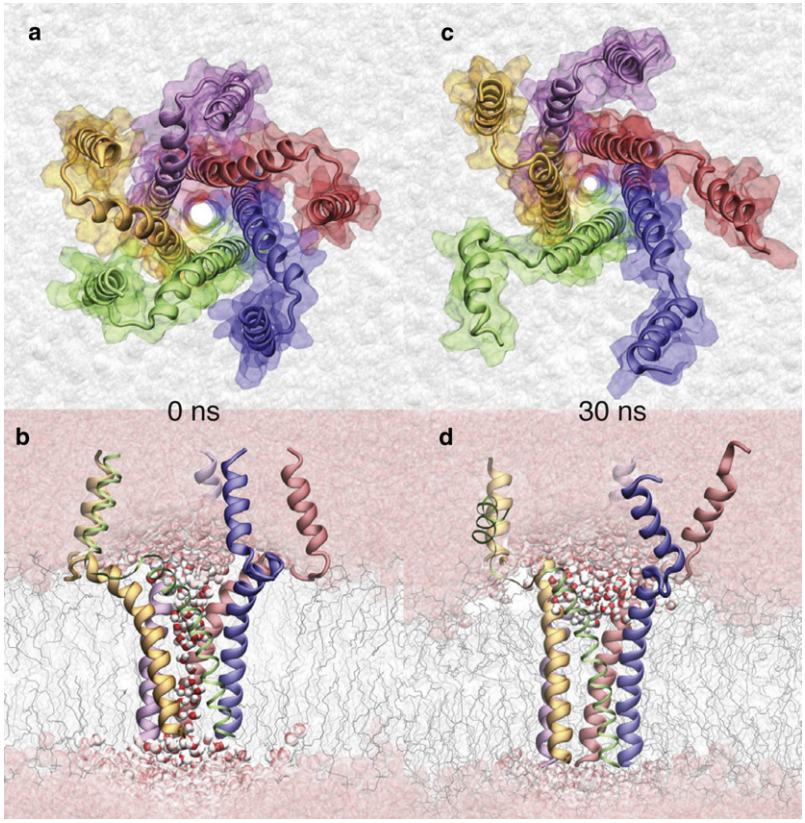

FIGURE 1 AA simulation of the bellflower pentamer embedded in a lipid bilayer membrane. (*a* and *b*) The conformation of the system at the beginning of the simulation. (*c* and *d*) The conformation of the system after a 30-ns MD simulation at constant pressure. The top and bottom rows provide views of the system from the cytoplasm and from the plane of the bilayer, respectively. The PLN pentamer is shown in cartoon representation and as a transparent molecular surface; the lipids are shown as lines; water near the pore is explicitly shown in the vdW representation; water molecules away from the pore are shown as semitransparent spheres.

CG methods

In the CGMD method, the degrees of freedom of the system are greatly reduced by clustering groups of atoms into beads; each bead corresponds to approximately four nonhydrogen atoms. Such clustering and the resulting smoothing of the potential energy function allow for a larger integration time step to be used in an MD simulation and allow for a substantial increase in computational speed at the expense of accuracy (29). In addition, the smoothed potential energy function results in diffusion rates that are around four times faster than AA diffusion rates (30). We account for this factor when reporting the duration of our CG simulations. CGMD simulations were shown to accurately reproduce phase properties of lipid-water systems (29). Recently, this approach was extended to protein-lipid systems (31).

In our CG simulations, we used the MARTINI force field (32) for dodecylphosphocholine (DPC) detergent, dioleoylphosphatidylcholine (DOPC) lipid, and water. For the protein, we used parameters developed by the Schulten group (31). CG systems were built by converting the corresponding AA system using the visual MD software package VMD (33). All CG simulations were performed using NAMD (22) and a 20-fs integration time step.

AA model of the bellflower pentamer in a lipid bilayer

The lowest energy conformation of the ensemble resolved by NMR (Protein Data Bank access code 1ZLL) was merged with a patch of a preequilibrated DOPC bilayer membrane. Lipids clashing with the protein were removed. The resulting system was solvated and ionized to a 0.12-M solution. The final system contained 146,785 atoms. This system was minimized for 3000 steps, heated to 310 K in 1-K increments over 31 ps by velocity rescaling, and equilibrated for 1.0 ns in the NPT ensemble, with all nonhydrogen atoms of the protein harmonically restrained to the NMR coordinates. Equilibration was continued for another 5.1 ns while applying the harmonic restraints to the protein backbone only. The system obtained at the end of the equilibration was used for subsequent unrestrained simulations in which the pressure in the plane of the bilayer was maintained using different methods (see Results and Table 1).

AA and CG models of the bellflower pentamer in a detergent micelle

A CG model of the protein-detergent system was built from a corresponding AA model of the bellflower pentamer (18). In the initial conformation, the PLN pentamer was surrounded by 300 DPC molecules randomly distributed in a 48.5-Å-tall cylinder with a radius of 30 Å. The system was solvated and ionized to 0.12 M with Cl^- and Na^+ ions. This AA system was converted into a CG system containing 14,886 CG beads. In the CG simulations, the protein conformation was fixed to the NMR coordinates and the molecules of detergent were allowed to self-assemble into a micelle. The CG system was minimized for 20 steps, heated to 310 K using the Langevin temperature control, and equilibrated for 23.2 ns, which was sufficient to observe the formation of a micelle around the protein. It is known from experiment that in water, DPC forms micelles containing 50–60 molecules (34). However, the number of DPC detergent molecules surrounding a membrane protein such as the PLN pentamer may be greater than the number of molecules in a pure micelle. Our attempts to build a CG model of a PLN pentamer micelle containing fewer than 300 DPC molecules (we used 65, 140, and 200 molecules) were not successful because DPC did not completely cover the transmembrane surface of the pentamer in the resulting structures. This result may have been caused by the inaccuracies in the CG force field.

To study structural fluctuations of PLN in a micelle, the CG model was reverse coarse-grained to an AA model using VMD (33). Before the procedure, DPC molecules whose headgroups were in close proximity (12 Å) to the hydrophobic transmembrane portion of PLN (58 molecules) were discarded to ensure that the micelle did not contain pathways to the interior lined by DPC headgroups.

The reverse CG procedure produced a system comprised of 158,564 atoms. After the conversion, the AA system was minimized for 8000 steps with all atoms of the protein fixed. Subsequently, the system was heated from 0 to 310 K in 10 ps using the Langevin temperature control, and equilibrated for 7.4 ns with all protein atoms restrained. Finally, all restraints were removed and the system was equilibrated for another 36.4 ns.

TABLE 1 Summary of all simulations performed

System	Model	Environ.	Ensemble	Method	Duration (ns)
Constant-ratio	bellflower	DOPC	NPT	AA	30
Constant-area	bellflower	DOPC	NAT/Np_zT	AA	17
Micelle	bellflower	DPC	NPT	CG/AA	23/36
Pinwheel	pinwheel	DOPC	NPT	AA	23/48
CG bellflower	bellflower	DOPC	NPT	CG	400/2100
CG pinwheel	pinwheel	DOPC	NPT	CG	580/360/2000
SMD	bellflower	DOPC	NVE	AA	16 × 1

AA model of a pinwheel pentamer in a lipid bilayer

A pair of AA systems were created by placing a PLN pentamer in the pinwheel conformation in a preequilibrated lipid bilayer patch containing 344 DOPC molecules. In the first system, the pentamer was placed in the bilayer by aligning its transmembrane region to the bellflower model. The second system was produced by moving the pinwheel pentamer 8 Å lower so that its cytoplasmic helices were in better contact with the bilayer. Each system was solvated to 0.12 M concentration of KCl electrolyte. The final systems each contained 146,785 atoms.

Each system was minimized for 5000 steps and heated to 310 K using Langevin temperature control. The systems were simulated with the protein coordinates harmonically restrained to the pinwheel coordinates for 2.5 ns. The resulting models were used as the starting conformations for production simulations lasting 22.6 ns and 48.2 ns.

CG models of bellflower and pinwheel pentamers in a lipid bilayer

To determine the stability of each model on a microsecond timescale, the initial AA systems containing either the pinwheel model (two configurations) or the bellflower model embedded in a DOPC bilayer were coarse-grained using the procedure described above. A fourth CG system contained the bellflower model and was built from the final frame of the AA, constant-ratio simulation of the bellflower model in a lipid bilayer. The resulting CG systems contained 12,616 and 12,621 CG beads for the pinwheel and bellflower models, respectively.

After a 4000-step minimization and 0.5-ns simulation with restraints applied to the protein backbone, production simulations were performed on the systems containing the bellflower and pinwheel models.

Ion transport through the bellflower model

Using the equilibrated AA model of the bellflower pentamer embedded in a lipid bilayer membrane, four smaller (81 Å × 81 Å × 95 Å) systems were constructed by removing lipid and water molecules from the periphery of the system. In each system, a single Ca^{2+} or Cl^- ion was placed near the entrance of the pore. The ion concentration in each system was adjusted to 0.1 M. The resulting system was minimized for 10,000 steps, heated, and allowed to equilibrate in the NPT ensemble for 0.2 ns with the protein and the ion near the pore entrance harmonically restrained to the initial coordinates. The conformation of the PLN pentamer used for the ion conductance studies was very close (root mean-square deviation (RMSD) of <1 Å for the backbone atoms) to that of the NMR model.

Following the procedure of Anishkin and Sukharev (35), steered MD (SMD) simulations were performed in the *NVE* ensemble (constant number

of atoms (N), volume (V), and energy (E)) to pull ions through the pore of the pentamer. The ion of interest was harmonically restrained ($k_{spring} = 69.5$ pN/Å) to a plane parallel to the bilayer. The plane was moved at a constant velocity of 30 Å/ns along the pore of the pentamer. The force exerted on the ion was recorded every 0.1 ps. From the dependence of the force on the location of the ion, the potential of mean force (PMF) was estimated by assuming that the dissipative force is directly proportional to the average ion velocity, and that the free energy of the system before and after the ion translocation is the same (36). The α-carbon atoms of the protein were harmonically restrained in the direction normal to the bilayer to prevent a lateral drift of the protein while allowing the pore to change its shape. Four separate SMD simulations were performed on each system.

RESULTS AND DISCUSSION

We begin this section by describing simulations of a PLN pentamer starting from the bellflower conformation embedded in three different hydrophobic environments, followed by a brief outline of the main results. Next, we provide a detailed comparison of the dynamics seen in the three simulations. We describe the outcome of AA simulations of the pinwheel model in a lipid bilayer, and then microsecond CG simulations of bellflower and pinwheel pentamers in a lipid bilayer. Finally, we describe the fourth set of simulations, in which ions were forced to move through the pore of the pentamer. Table 1 summarizes all simulations performed.

AA simulations of the bellflower model in different hydrophobic environments

Constant-ratio lipid bilayer simulation

Fig. 1, *a* and *b*, shows the microscopic model of the PLN pentamer in the bellflower conformation embedded in a DOPC bilayer. Fig. 1 *b* explicitly shows the water molecules that were initially placed inside the pore of the pentamer. Starting from this conformation, the model was equilibrated in the NPT ensemble, with the protein restrained for 6.1 ns. Within 200 ps from the beginning of the simulation, water molecules exited the pore, with no water molecules entering the pore from the bulk. Water molecules were not observed entering the pore in any of the subsequent equilibration simulations. These simulations clearly demonstrate that the pore of the bellflower pentamer does not retain water.

After the restrained equilibration, the simulation was continued for 30.7 ns without restraints. In this simulation, the NPT ensemble was maintained using a barostat that constrained the dimensions of the bilayer to a constant ratio. Fig. 1, *c* and *d*, shows the state of the system after the equilibration. A comparison of the initial and final states reveals that the pore of the pentamer shrank during the course of the simulation and the overall conformation of the bellflower pentamer became asymmetric. Using the package HOLE (37), we found that the minimum radius of the pore was reduced from 1.92 to 1.29 Å.

Constant-area lipid bilayer simulation

MD simulations using the CHARMM force field sometimes fail to reproduce the experimentally measured density of lipid bilayers when isotropic pressure control is used (38). Common remedies to this problem are to apply tension in the plane of the bilayer or to fix the area of the lipid patch at the experimental value. To verify that the observed asymmetry of the bellflower pentamer is not an artifact of the force field used, we performed a constant-area simulation of the PLN pentamer. The starting conformation for this simulation was prepared by increasing the size of the membrane patch in small increments (0.5 Å every 0.1 ns). During this procedure, the protein conformation was restrained as the area/lipid increased from 66 Å^2 to the experimentally measured value of 72 Å^2 (39). The lipid density was measured by counting the number of lipid headgroups inside a region that excluded a square patch centered around the protein (70 Å on each side). Subsequently, all restraints were released, and the system was equilibrated for 13.4 ns. The area in the plane of the lipid bilayer was fixed, whereas the size of the system normal to the lipid bilayer was allowed to fluctuate according to the NPT ensemble. In accord with our previous observations, the pore of the pentamer shrank to an average minimum radius of 1.41 Å, whereas the conformation of the bellflower pentamer became asymmetric. The upper portion of the transmembrane region developed three kinks around Asn^{30}, but the lower transmembrane region remained stable.

Micelle simulation

To determine whether the bellflower model is stable in the hydrophobic environment of the NMR experiment, we built a CG model containing DPC detergent and the PLN pentamer and simulated the self-assembly of DPC detergent into a micelle about the fixed pentamer. Fig. 2, *a* and *b*, illustrates the self-assembly process. Fig. 2, *c* and *d*, shows

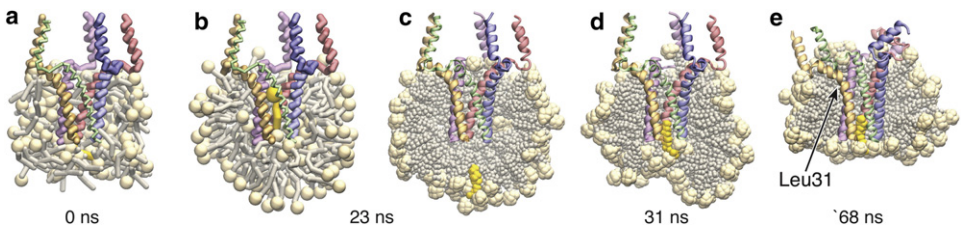

FIGURE 2 AA and CG simulation of the bellflower pentamer in a micelle. (*a*) Start of the CG simulation: PLN is surrounded by randomly arranged DPC molecules. (*b*) The outcome of the CG simulation: a micelle is formed around the PLN pentamer. (*c*) AA model of the configuration shown in *b* after brief annealing. (*d*) AA system at the moment when all restraints are removed. (*e*) The final frame of the AA simulation. Molecules of detergent in front of the protein are not shown. The molecules of detergent inside the transmembrane pore of the PLN pentamer are shown in yellow.

further evolution of the micelle after the CG model was converted to an AA representation. Fig. 2, *d* and *e*, depicts the system before and after a 36-ns unrestrained AA equilibration, during which the transmembrane helices developed an asymmetry, and the pore shrank to an average minimum radius of 1.48 Å. Fig. 2 *e* also points out a kink in a transmembrane helix at Leu^{31} that developed shortly after restraints were released and persisted for the duration of the simulation.

During the course of the CG simulation, one DPC molecule, highlighted in yellow in Fig. 2, *a* and *b*, entered the pore of the pentamer from the lumen in a head-first orientation. This detergent molecule was removed when the CG model was converted to AA. However, after 1 ns of the AA simulation, a different DPC molecule (Fig. 2, *c–e*, *yellow*) entered the pore tail first from the lumen side of the pore. These simulations suggest that the pore of the pentamer is likely blocked by a detergent molecule, the coordinates of which could not be resolved by NMR.

Conformational dynamics of the bellflower model

To better understand the structural changes that took place during the above simulations, we first characterized the dynamics of individual protomers in the pentamer. Fig. 3 *a* plots the average RMSD of the protein backbone from the coordinates resolved by NMR for the cytoplasmic (residues 1–16) and transmembrane (residues 22–52) helices, and for the entire protomer (residues 1–52). The RMSD was calculated by aligning each structural element of a protomer to the NMR structure. The RMSD for each of the five protomers was averaged to produce the data shown in Fig. 3 *a*. The standard deviation from the average over the five protomers was ~1, 0.3, and 0.4 Å for the entire protomer, the cytoplasmic region, and the transmembrane region, respectively.

Fig. 3 *a* shows that the RMSDs of both helical regions converge to the same value in all simulations within the first 2 ns, whereas the RMSD of the entire monomer does not reach a constant value. Thus, we conclude that individual α-helices of PLN protomers do not undergo major conformational changes, whereas the structure of the entire pentamer does.

Below, we provide a detailed analysis of the conformational transformations taking place in the cytoplasmic and transmembrane domains of the protomers.

Structural changes in the cytoplasmic region

Fig. 3 *b* shows per residue root mean-square fluctuation (RMSF) of the backbone's coordinates. The RMSF was calculated for each of the two α-helices of a protomer after independently aligning each helix to the NMR structure. The RMSF was averaged over the five protomers at each residue to produce the data shown in Fig. 3 *b*.

Visual analysis of the MD trajectories revealed that the largest structural fluctuations, which occurred in the micelle simulation, correspond to the formation of kinks in the cytoplasmic helices of two adjacent protomers. Residues 13–16 of one cytoplasmic helix were observed to unwind, allowing this helix to reach a neighboring cytoplasmic helix and form a bound state that lasted for 14 ns. The helices crossed almost orthogonally such that the majority of the hydrophobic residues were exposed to the solution. The binding interaction was dominated by hydrophobic and coulombic forces between Thr^8 and Thr^8, hydrophobic forces between Thr^8 and Val^4, and hydrophobic forces between Gln^5 and Val^4.

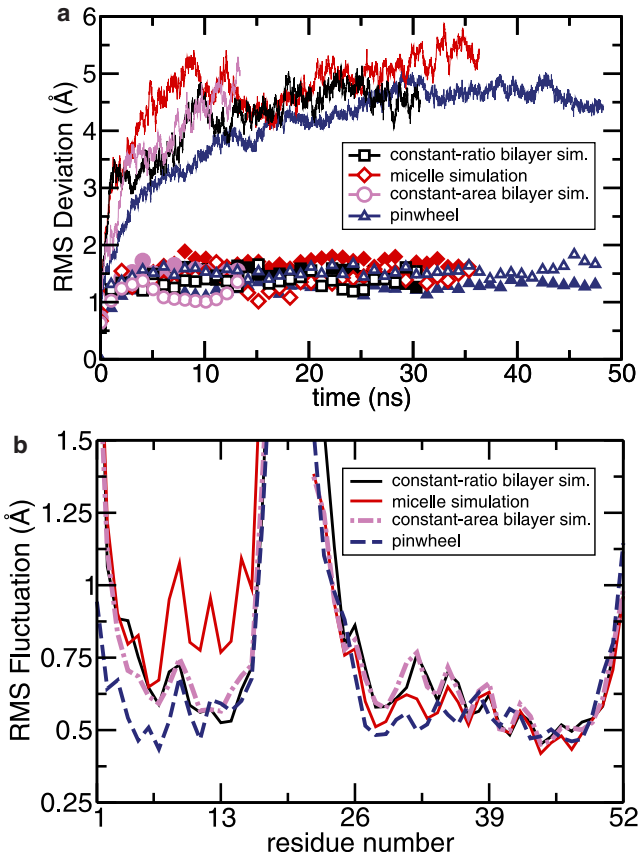

FIGURE 3 Conformational fluctuations of the PLN protomers. (*a*) Average RMSD of the backbone atoms from the NMR coordinates shown for the entire protomer (*lines*) and the cytoplasmic (*open symbols*) and transmembrane helices (*solid symbols*). (*b*) Average RMSF of the backbone atoms computed over the unrestrained trajectories. Cytoplasmic (residues 1–16) and transmembrane helices (residues 22–52) were independently aligned to the corresponding NMR structures. Data resulting from four MD simulations are shown (see text).

The α-helical structure of two other cytoplasmic helices was observed to transiently break about Arg^9 during the micelle simulation, and the helices were observed to bend about this residue. Similar deformations of cytoplasmic helices were observed during the constant-area simulation about residue Thr^8 and during the constant-ratio simulation about Tyr^6. The latter deformation occurred while two neighboring cytoplasmic helices transiently formed a bound state. The above observations are consistent with the proposal that the high

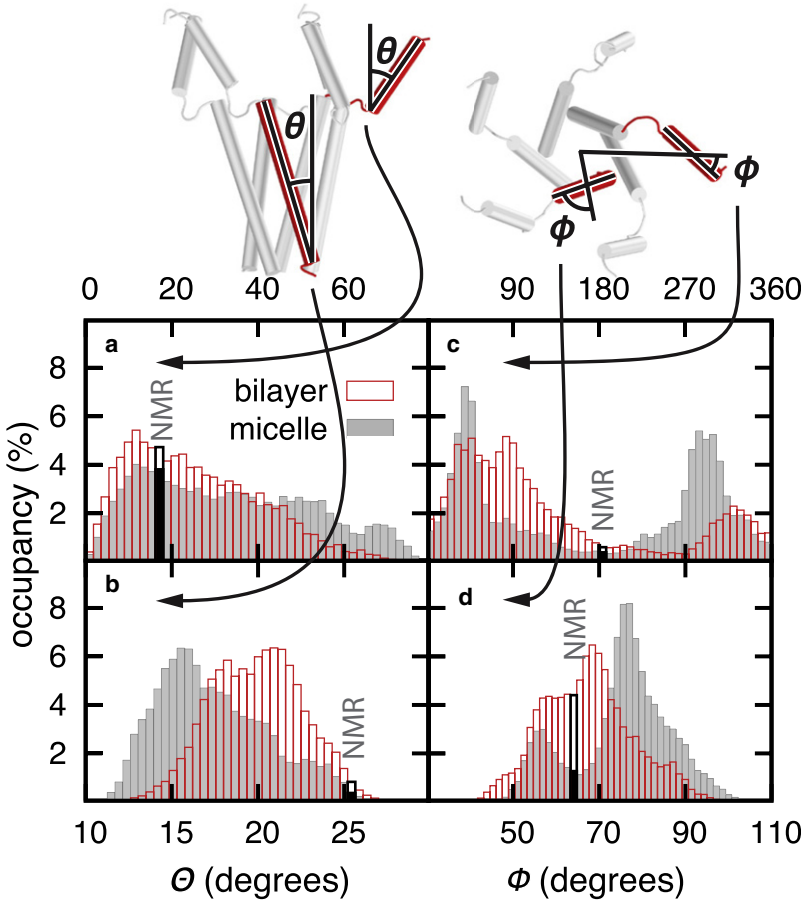

FIGURE 4 Orientation of the PLN helices in the AA simulations of the bellflower pentamer. (*a* and *b*) Histogram of the angle, θ, between the cytoplasmic (*a*) and transmembrane (*b*) helices and the axis of the pore. (*c* and *d*) Histogram of the angle ϕ between the axis of the cytoplasmic (*c*) and transmembrane (*d*) helices and the radial vector passing from the center of the pore and the center of mass of the helix. The insets above the graph illustrate the definitions of the angles. The angles from the NMR structure are labeled in the panels. The occupancy is defined as the fraction of time the helix occupies a given range of angles during each simulation. Data for the micelle and constant-ratio bilayer simulations are shown as solid and open histograms, respectively.

flexibility of this region facilitates recognition between PLN and a variety of other proteins such as SERCA, protein kinase A, and cyclic AMP-dependent protein kinase (7).

Fig. 4, *a* and *c*, characterizes the orientation of the cytoplasmic helices. For each helix, we plot the angle, θ, between the helix and the axis of the pore of the pentamer. Fig. 4 *a* shows that the peak of the distribution of the angle θ in the constant-ratio and micelle simulations is close to the value calculated from the NMR structure (18). However, the distribution is spread out, indicating that, on average, the helices lay closer to the plane of the bilayer than suggested by the NMR structure. None of the cytoplasmic helices laid close enough to the plane of the bilayer to interact directly with the lipids or detergent surrounding the transmembrane region, as suggested by the pinwheel model.

For each helix, we computed the angle, ϕ, between the radial vector extending from the center of the pentamer to the center of mass of the helix and the axis of the helix, both projected into the plane of the bilayer. Fig. 4 *c* shows that in both bilayer and micelle simulations, the orientation of the cytoplasmic helices resolved by NMR (18), i.e., pointing toward the pore, is among the least likely. The cytoplasmic helices are most likely to point away from the pore, at ~45° to either side of the radial direction. We conclude thereby that the orientation of the cytoplasmic helices resolved by NMR in Oxenoid and Chou (18) does not represent a typical conformation of a PLN pentamer observed in our simulations.

Fig. 5 *a* shows the range of conformations explored by the cytoplasmic helices in the constant-ratio simulation. The figure was made after aligning the transmembrane region at each time step to the NMR structure.

Structural changes in the transmembrane region

The orientation of the transmembrane helices is characterized in Fig. 4, *b* and *d*, using angles ϕ and θ, defined above. Fig. 4 *b* indicates that the orientation of the transmembrane helices with respect to the pore axis in the NMR structure (18) is quite close to the average orientation observed in our simulations. Nevertheless, the helices in the NMR structure are oriented ~5° closer to the plane of the bilayer than in our MD simulations. Also, the helices in the bilayer simulation are oriented closer to the plane of the bilayer than in the micelle simulation, with the exception of one helix in the micelle system. The latter helix became kinked at Leu^{31} (see Fig. 2 *e*) within the first nanosecond of the simulation and remained kinked throughout the simulation.

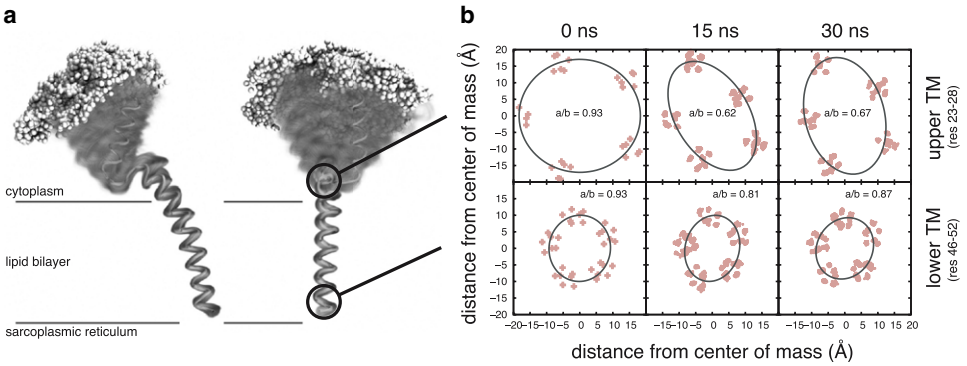

FIGURE 5 Structural fluctuation of the bellflower pentamer. (*a*) Superposition of conformations assumed by the PLN protomers over the course of the 30.7-ns constant-ratio simulation. The transmembrane region of each protomer is aligned. The N-terminus α-carbon atom is shown every 0.1 ns as a vdW sphere, and the rest of the protein is shown in a transparent cartoon representation every 0.01 ns. Finally, a protomer in the original bellflower conformation is shown in an opaque cartoon representation. (*b*) Asymmetry of the transmembrane region of the pentamer. Coordinates of the α-carbon atoms in the upper (*upper*) and lower (*lower*) transmembrane regions are plotted alongside the best-fit ellipse for the constant-ratio simulation. To make the plots in *b*, the transmembrane region of the pentamer was aligned to the NMR structure. Coordinates of the α-carbon atoms were projected onto the plane of the bilayer. An ellipse was fit to the set of coordinates obtained during the 0.5-ns interval immediately after the states obtained after 0, 15, and 30 ns of the simulation. The ratio of the minor to major axes of the best-fit ellipse is shown for each time interval.

Within the first nanosecond of the constant-area simulation, kinks formed around Asn^{30} in three protomers and persisted for the duration of the simulation. In contrast, no kinks were observed in the constant-ratio simulation. Unlike the kinks observed in the cytoplasmic helices, the kinks in the transmembrane helices did not contribute to the RMSF, because the kinks remained stable. The presence of the kinks in the transmembrane helices near residue Asn^{30} qualitatively agrees with the electron paramagnetic resonance data, which showed that the transmembrane region above residue Asn^{30} is dynamic on a microsecond to millisecond timescale and the transmembrane region below residue Asn^{30} is not (7).

In all simulations, the transmembrane helices that did not form kinks straightened from a 37° bend to an average bend of ~20° in the constant-ratio and 10° in the micelle simulations. For comparison, the pinwheel model (19) depicts a 9.2° bend.

Kinks in the transmembrane helices of PLN protomers make the conformation of the entire pentamer asymmetric. However, careful examination of Fig. 1 *c* reveals that asymmetry also developed during the constant-ratio simulation where no kinks formed in the transmembrane helices. To characterize the asymmetry of the upper (residues 23–28) and lower (residues 46–52) transmembrane regions of the pentamer, an ellipse was fit to the coordinates of each region. Fig. 5 *b* plots the best-fit ellipse to the coordinates of the upper and lower transmembrane regions at various times during the constant-ratio simulation. The ratio of the minor to major axes of the best-fit ellipse fluctuates around 0.65 for the upper transmembrane part of the pentamer, indicating a strong deformation of the pore. The best-fit ellipse is nearly circular in the lower transmembrane region. Similar analysis carried out for the constant-area and micelle simulations revealed that the axis along which the symmetry is broken in the upper transmembrane region is different in each simulation (data not shown). Fluctuating asymmetry has also been observed in the transmembrane region of α-hemolysin (40) and the mechanosensitive channel of small conductance (41). The authors of the latter article suggest that the observed asymmetry may entropically enhance the transmembrane region's stability by allowing it to occupy "a larger conformational space than a single symmetric conformation". However, in all simulations, the lower transmembrane region remained highly stable and showed very little asymmetry.

AA simulations of the pinwheel model in a lipid bilayer

Initially, the pinwheel model was placed in a DOPC bilayer by aligning its transmembrane region to that of the bellflower model. In that conformation, the cytoplasmic helices just barely contacted the bilayer. During the 23 ns of unrestrained AA simulation in the NPT ensemble, three of the cytoplasmic helices lost their contact with the bilayer and moved upward, away from the bilayer.

The second AA model of the pinwheel system was built to ensure good initial contact between the bilayer and the cytoplasmic helices. In the initial structure, the C-terminal α-carbons of the pentamer's transmembrane region were located 9 Å below the phosphorus atoms of the lower leaflet, whereas the N-terminal residues were deeply embedded in the headgroups of the upper leaflet (Fig. 6 *b*). Within 20 ns from the beginning of the simulation, the pentamer shifted by 10.5 Å relative to the bilayer, and the upper transmembrane region (residues 22–26) emerged from the opposite side of the bilayer. Furthermore, the bilayer became curved (convex from the cytoplasm) so that the cytoplasmic helices, which remained firmly tethered to the bilayer, inclined toward the bilayer (Fig. 6 *d*). This simulation trajectory is used in the following analysis.

The RMSD analysis shown in Fig. 3 *a* indicates that the structure of the protomers in the pinwheel and bellflower

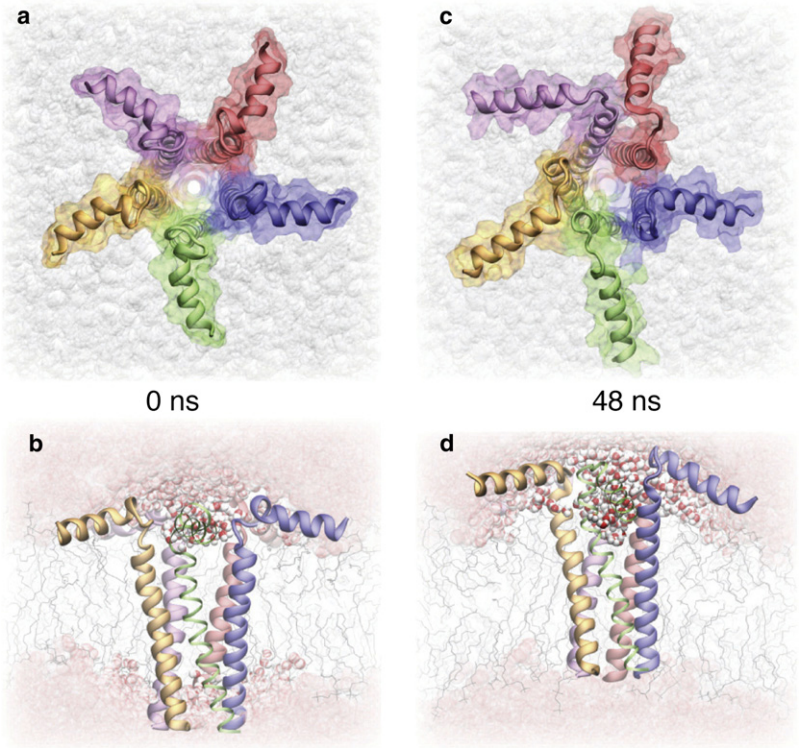

FIGURE 6 AA simulation of the pinwheel PLN pentamer embedded in a lipid bilayer membrane. (*a* and *b*) The conformation of the system at the beginning of the simulation. (*c* and *d*) The conformation of the system after a 48-ns MD simulation at constant pressure. The top and bottom rows provide views of the system from the cytoplasm and from the plane of the bilayer, respectively. The PLN pentamer is shown in the cartoon representation and as a transparent molecular surface; the lipids are shown as lines; water near the pore is explicitly shown in the vdW representation; water molecules away from the pore are shown as semitransparent spheres.

models deviate from their initial conformations to the same degree, on average. In a similar way, Fig. 3 *b* shows that the RMSF values observed in the simulations of the pinwheel model are generally lower than that of the bellflower model. Although the pinwheel model was constructed from coordinates of monomeric PLN resolved by NMR, the RMSF and RMSD for the pinwheel model are about the same as or smaller than those for the bellflower model, particularly in the transmembrane region, where protein-protein interactions are significant.

Fig. 7 shows the angles θ and ϕ assumed by the transmembrane and cytoplasmic helices in the AA simulation of the pinwheel model (the angles are defined in Fig. 4). The initial orientation of the transmembrane helix was the most likely orientation observed during the simulation. Likewise, the radial arrangement of the cytoplasmic helices was maintained throughout the simulation, except in the case of one helix (see Fig. 6 *c*). Nevertheless, the cytoplasmic helices were observed to incline toward the bilayer (Fig. 7, *e* and *f*). We attribute this motion to the relative displacement of the bilayer and the transmembrane helices, which pushed the base of the cytoplasmic helices (residue 16) away from the bilayer. Comparing the distributions in Fig. 7, *c* and *d*, to those in Fig. 4, *c* and *d*, reveals that the

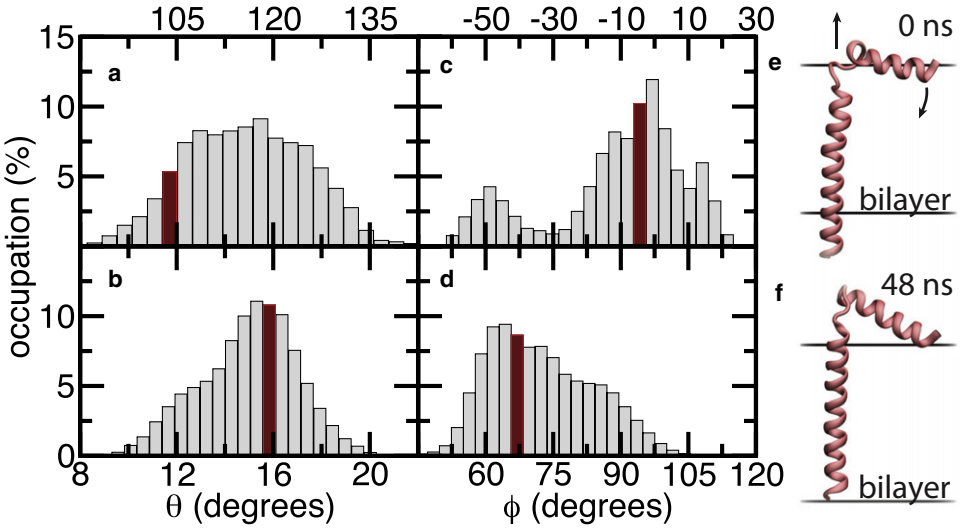

FIGURE 7 Orientation of the PLN helices in AA simulations of the pinwheel pentamer. (*a* and *b*) Histogram of the angle θ between the cytoplasmic (*a*) and transmembrane (*b*) helices and the axis of the pore. (*c* and *d*) Histogram of the angle ϕ between the axis of the cytoplasmic (*c*) and transmembrane (*d*) helices and the radial vector passing from the center of the pore and the center of mass of the helix. (*e* and *f*) Typical conformations of the pinwheel protomer at the beginning (*e*) and end (*f*) of the AA simulation. The angles and occupancy are defined in Fig. 4. The starting value of the angles (the pinwheel model) are shown in dark red.

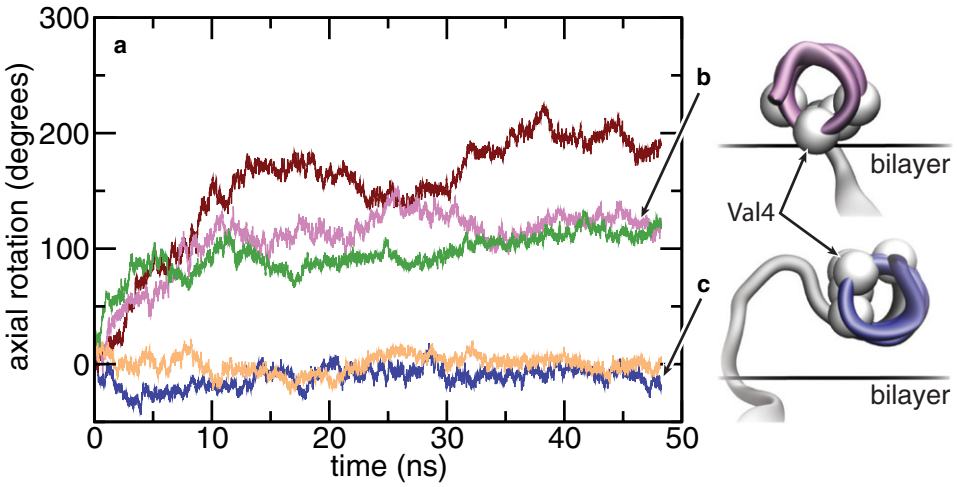

FIGURE 8 Axial rotation of the cytoplasmic helices in the pinwheel model. (*a*) Time series of the axial angle for each protomer. (*b* and *c*) Representative conformations of the cytoplasmic helices at the end of the simulation are shown along the corresponding helical axes. The α-carbon atoms of the hydrophobic residues are shown as white spheres. The line indicates the approximate position of the bilayer defined by the location of its phosphorus atoms within 10 Å of the protein. Note that the bilayer is curved near the protein (see Fig. 6 *d*).

transmembrane helices in the bellflower and pinwheel models assume similar orientations in a lipid bilayer. Furthermore, the transmembrane helices of the pinwheel model bend compared to the initial structure, averaging 13.1° in the last 30 ns of simulation.

Fig. 8 illustrates the rotation of the cytoplasmic helices about their helical axes: The axial angle (defined below) of each helix is plotted versus time. To measure the angle, rotations in θ and ϕ (defined in Fig. 4) were applied to the helix's coordinates, which aligned the helix with its conformation in the original pinwheel model. The applied rotations were such that the helix experienced no rotation about its own axis, which is required for the measurement of the axial angle. The axial rotation angle was then extracted using a least-squares fit to the α-carbon atom coordinates in the original pinwheel model. Fig. 8 shows that only two out of five helices maintained the same axial orientation throughout the simulation, whereas the other three helices rotate about their axes to 90–180°. Here, a positive rotation angle corresponds to a clockwise rotation of the helix when looking down its axis from the N-terminus. In the pinwheel model, the hydrophobic face of each cytoplasmic helix is oriented at nearly 90° to the bilayer. During the simulation, only three of the helices rotated so that the hydrophobic face came in closer contact with the lipid bilayer. These data illustrate that the interaction between the cytoplasmic helices and the bilayer is not purely hydrophobic; the two helices that maintained the initial angle were tethered by electrostatic interactions between the charged and polar residues of the protein and the polar groups of the lipid bilayer.

Although the transmembrane region of the pinwheel model exhibits relatively low RMSD and RMSF, the overall conformation of the pinwheel pentamer becomes asymmetric, as in the case of the bellflower model. The ratios of the minor to major axes of the best-fit ellipse to the coordinates of the upper and lower transmembrane regions (data not shown) are similar to those observed in the simulation of the bellflower model (see Fig. 5).

CG simulations of the pinwheel and bellflower models in a lipid bilayer

CGMD simulations were performed so that we could observe the evolution of the pinwheel and bellflower models on a microsecond timescale.

Three CG simulations of the bellflower pentamer were performed. First, two simulations were performed on a CG system constructed from the final frame of the AA, constant-ratio simulation of the bellflower model (Fig. 1, *c* and *d*). In both simulations, the same two pairs of cytoplasmic helices formed a bound state, whereas the fifth helix came into contact with the bilayer. These events occurred within 74 ns in one simulation and 264 ns in the other. The resulting conformations remained stable for the duration of the simulations (580 and 360 ns, respectively). Another 2.0-μs CG simulation of the bellflower pentamer was performed starting from the coordinates of the original bellflower model (Fig. 9 *a*). Fig. 9, *b* and *c*, illustrates the conformation obtained at the end of the simulation. During the first 80 ns of the simulation, four of the cytoplasmic helices came into contact with the bilayer, arranging in a clockwise direction when viewed from the cytoplasm. Each helix that came into contact with the bilayer also interacted with the upper transmembrane region or the loop of the adjacent protomer, except for one helix that interacted with the cytoplasmic helix of the protomer that did not come into contact with the bilayer (Fig. 9, *b* and *c*). The overall configuration of the cytoplasmic helices did not change significantly through the rest of the simulation. The transmembrane region became highly asymmetric just after the beginning of the simulation and tilted as a whole away from the bilayer's normal.

The NMR studies of the PLN pentamer showed a single set of chemical-shift resonances and suggested a symmetric structure of the pentamer (18,21). If the asymmetric conformations observed in our simulations persist over the mixing time of the NMR measurement, multiple peaks should be observed in a 2D NMR spectrum. This apparent

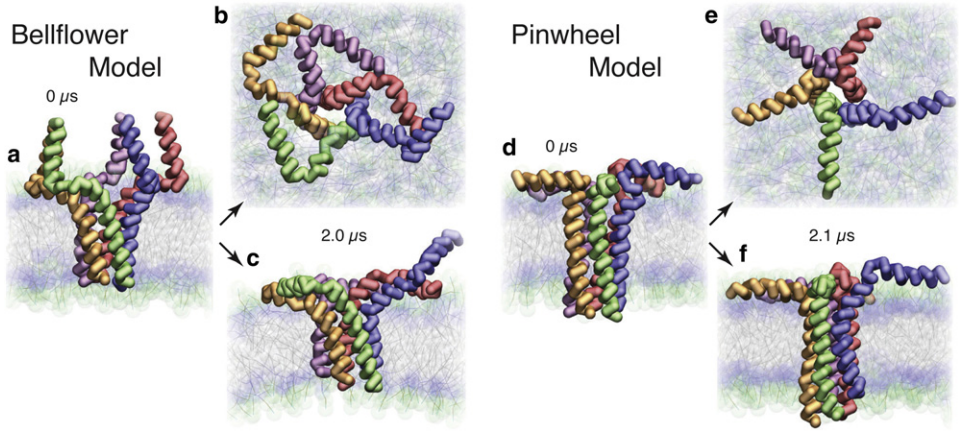

FIGURE 9 CG simulations of the bellflower (*a–c*) and pinwheel (*d–f*) pentamers in a lipid bilayer membrane. (*a* and *d*) The conformation of the systems at the beginning of the simulations shown from the plane of the bilayer. (*b*, *c*, *e*, and *f*) The conformation of the systems at the end of the CGMD simulations shown from the cytoplasm (*b* and *e*) and from the plane of the bilayer (*c* and *f*). The bilayer is shown as transparent spheres and solid lines colored according to the bead types. The protein backbone is shown as beads connected by bonds.

disagreement between NMR and our MD study could be reconciled if thermal fluctuations average the axis of the ellipse shown in Fig. 5 *b* over each subunit during the course of the mixing time in an NMR measurement. Such prominent fluctuations were not observed during our simulations, but have been observed in simulations of other oligomers (40,41).

Two CG simulations of the pinwheel pentamer were performed. First, a 400-ns CG simulation was carried out, starting from the system that had the cytoplasmic helices of the pentamer only loosely in contact with the bilayer (see previous section). Within the first 56 ns, the same three cytoplasmic helices that lost contact with the bilayer in the AA simulation lost contact with the bilayer in the CG simulation; these contacts were not reestablished during the remainder of the simulation. The second 2.1-μs CG simulation was carried out, starting from the system that had the pinwheel pentamer deeply embedded in the lipid bilayer (Fig. 9 *d*). Fig. 9, *e* and *f*, depicts the conformation of the pinwheel model at the end of the simulation. Within the first 56 ns, the cytoplasmic helices rotated so that each hydrophobic face came into contact with the bilayer and remained bound to the bilayer throughout the simulation. Unlike the transmembrane region of the pinwheel model in the AA simulation, most of the N-terminal side of the transmembrane region remained exposed to the electrolyte, with the exception of one helix (the rightmost protomer in the foreground of Fig. 9 *e*). This transmembrane helix became bent in a manner reminiscent of the bend seen in the original bellflower model. The C-terminus of that same protomer extended by 5 Å away from the pentamer's center. Thus, AA and CG simulations of the same pinwheel system predict a somewhat different arrangement of the lipid bilayer around the pentamer. This difference might originate from the imperfections of the CG model; the AA model is expected to be more accurate as it uses a considerably more detailed and well-tested force field. Thus, we advise caution when interpreting results of CG simulations.

From these CG simulations, we conclude that it is very likely for the cytoplasmic helices of a PLN pentamer to contact the surface of a lipid bilayer. At the same time, the interactions between charged residues of the adjacent protomers can have a considerable influence on the conformation of the cytoplasmic region, and tangential arrangement of the cytoplasmic helices (Fig. 9 *b*) is one possible conformation.

Ion conductance of the bellflower model

To determine the feasibility of Ca^{2+} or Cl^- ion transport through the pore of a PLN pentamer, Ca^{2+} and Cl^- ions were pulled in either direction through the pore using standard protocols of SMD (42). Fig. 10 *a* plots the force applied to the ion during each SMD run against the location of the ion in the pore. For most of each simulation trajectory, the SMD force was observed to point along the direction of ion transport. The maximum absolute value of the force was on the order of hundreds of piconewtons and was comparable for ion transport in both directions. However, the force plots exhibit significant hysteresis because of the pair of constrictions formed by residues Ile^{40} ($z \approx 0$ Å) and Leu^{44} ($z \approx -5$ Å) in the middle of the pore.

In a typical run, a trailing column of water two to four molecules in diameter formed as an ion was pulled through the pore. The translocation of ions was observed to halt in the pore upon encountering the first constriction. The translocation resumed after the SMD force had become sufficient to push the ion and its partial solvation shell through the constrictions. After passing through the constrictions, the trailing column of water narrowed to a chain of one to two water molecules in diameter. In the final stage of the translocation process, a chain of water was observed to form and connect the ion to the bulk water at the destination side of the membrane. As the ion exited the pore, the SMD force was observed to point toward the ion's starting point. Subsequently, the chain of water connecting both sides of the pore was observed to break and leave the pore.

Fig. 10 *a* shows that the force required to pull a Ca^{2+} ion through the pore is much larger than that to pull a Cl^- ion. Ca^{2+} ions are more charged and carry a larger, less flexible solvation shell than Cl^- ions (six molecules for Ca^{2+}, three to five for Cl^-). Hence, Ca^{2+} ions encounter greater

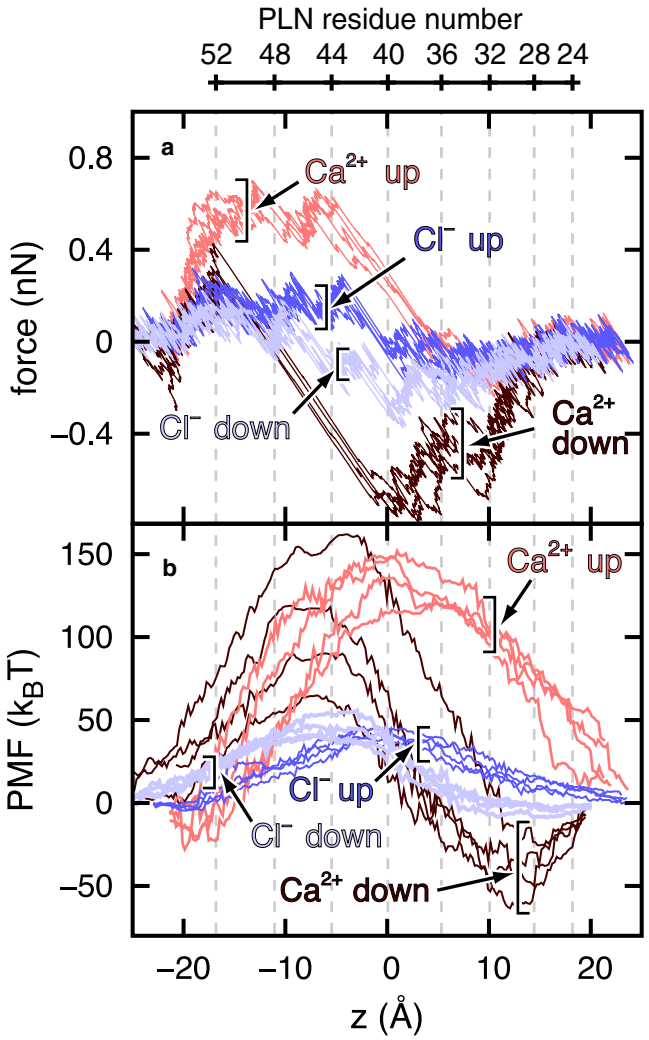

FIGURE 10 SMD simulations of ion transport through the pore of PLN (bellflower model). (*a*) SMD force applied to Cl^- and Ca^{2+} ions versus distance for each of the 16 SMD simulations. (*b*) Approximate PMF for each simulation, calculated according to the approach of Anishkin and Sukharev (35) and using data shown in *a*. The center of the transmembrane region of the protein lies at $z = 0$. Positive values of z indicate locations closer to the cytoplasm. Data labeled "up" and "down" correspond to ion transport from the SR to the cytoplasm and vice versa.

electrostatic and steric forces as they move through the pore. Consequently, the Cl^- ions were observed to move at a steadier pace through the pore, dwelling at the constrictions for only a short time.

Fig. 10 *b* shows an estimate of the PMF, which was calculated from the data of the SMD force versus location. The PMF was calculated by assuming that irreversible work was performed on the ion in the process of ion translocation. The coefficient of friction for the dissipative force was tuned to equate the free energy of the system before and after the transport event. The average coefficient of friction was 4.9 pN ns/Å for Ca^{2+} ions and 0.66 pN ns/Å for Cl^- ions. The peak PMF for Ca^{2+} and Cl^- transport ranged from 50 to 150 k_BT and 35 to 50 k_BT, respectively. Because the PLN pentamer does not retain water, and because the energetic barriers associated with ion translocation are orders of magnitude greater than k_BT, the PLN pentamer in the conformation resolved by NMR (18) is not expected to function as an ion channel. Although the above simulations were performed using the bellflower model, we expect that their main conclusion—that the potential energy barrier is too large for the PLN pentamer to function as an ion channel—also applies to the pinwheel model, because the transmembrane pore of the pinwheel model is even smaller than that of the bellflower model.

CONCLUSIONS

AA and CG models of a PLN pentamer in the bellflower and pinwheel conformations were simulated in a lipid bilayer membrane to investigate structural fluctuations and the preferred equilibrium conformation of the pentamer.

In the AA simulations of the bellflower model, the cytoplasmic helices, which initially pointed upward and toward the pore center (see Fig. 1 *b*), were found to point away from the center at a random angle with respect to the pore axis (see Figs. 4, *a* and *c*, and 5 *a*). Transient kinks and partial unwinding were abundant in the cytoplasmic helices of the bellflower pentamer, which is in agreement with mutagenesis studies suggesting that the cytoplasmic helices unwind (8,9). In these simulations, the cytoplasmic helices were not observed to come into contact with the lipid bilayer as depicted in the pinwheel model, but this may be due to the relatively short (~50-ns) timescale of our AA simulations. In the CG simulations of the same model, cytoplasmic helices were observed to come into contact with the bilayer, but instead of extending radially, as portrayed in the pinwheel model, the helices arranged tangentially around the pentamer (see Fig. 9 *b*). This tangential arrangement was stabilized by the interactions between the terminus of each cytoplasmic helix and the adjacent protomer's loop region. In the other two CG simulations of the bellflower pentamer, only one cytoplasmic helix came into contact with the bilayer, whereas the other four came into contact with one another in two pairs and remained immersed in the electrolyte. Similar bound states between adjacent cytoplasmic helices were observed in AA simulations of the bellflower model. Thus, in our simulations, the bellflower model did not represent the most probable conformation of the PLN pentamer. In accordance, a recent simulation study involving the bellflower pentamer embedded in a palmitoyloleoylglycerophosphocholine lipid bilayer membrane showed that the cytoplasmic domain of each protomer moved toward the bilayer surface (43).

The stability of the pinwheel model in AA and CG simulations depended on how deeply the pentamer was embedded in the bilayer at the onset of the simulation. In both AA and CG systems, when the transmembrane region of the

pinwheel pentamer was initially aligned to the transmembrane region in the bellflower model, three of the cytoplasmic helices rose toward the cytoplasm, making the pinwheel conformation unstable. When the pinwheel pentamer was placed 8 Å lower (see Figs. 6 *b* and 9 *d*), all cytoplasmic helices remained firmly tethered to the bilayer. Since this was the only simulation in which the initial conformation of the pentamer was, on average, preserved throughout the simulation, we conclude that a pinwheel conformation of the PLN pentamer is much more likely than a bellflower conformation. However, our simulations of the bellflower model suggest that the interactions between the cytoplasmic regions of the adjacent protomers should be taken into account in constructing a realistic model of a representative conformation of the PLN pentamer.

The lower transmembrane regions (residues 35–52) of the bellflower and pinwheel pentamers, which are similar (RMSD < 1.5 Å), remained very stable in our AA simulations. The overall conformation of the upper transmembrane region became asymmetric for both models (see Fig. 5 *b*). The upper transmembrane region of the AA bellflower model, which was initially curved away from the pore, was not maintained in any of the three hydrophobic environments used. Conversely, the transmembrane helices in the AA pinwheel model became slightly bent. This suggests that the most accurate conformation of the transmembrane region is intermediate between the pinwheel and bellflower structures. However, we can expect that the exact conformation depends on the hydrophobic environment. It is known, for example, that hydrophobic mismatch can induce a tilt (44) or bend (45) in membrane spanning helices; a thinner bilayer might providea structure more consistent with the bellflower model, and a thicker bilayer could produce a structure more consistent with the pinwheel model.

In response to reports suggesting the possibility of ionic conductance through PLN pentamers (4,5), we used SMD to simulate transport of Ca^{2+} and Cl^{-} ions through the pore of the bellflower pentamer. These calculations indicated that the free-energy barrier associated with Ca^{2+} or Cl^{-} ion translocation is on the order of tens of k_BT. The pore's inability to retain water and the large free-energy barrier associated with ion translocation indicate that in the conformation resolved by NMR (18), the PLN pentamer does not function as an ion channel.

This work is supported by grants from the National Institutes of Health (R01-HG003713 and PHS 5 P41-RR05969), the National Science Foundation (PHY0822613), and the Petroleum Research Fund (48352-G6). The authors gladly acknowledge supercomputer time provided by the National Center for Supercomputing Applications via a Large Resources Allocation grant (MCA05S028).

REFERENCES

1. Wegener, A. D., H. K. Simmerman, J. P. Lindemann, and L. R. Jones. 1989. Phospholamban phosphorylation in intact ventricles: Phosphorylation of serine 16 and threonine 17 in response to beta-adrenergic stimulation. *J. Biol. Chem.* 264:11468–11474.
2. Haghighi, K., K. N. Gregory, and E. G. Kranias. 2004. Sarcoplasmic reticulum Ca^{2+}-ATPase-phospholamban interaction and dilated cardiomyopathy. *Biochem. Biophys. Res. Commun.* 322:1214–1222.
3. Cornea, R. L., J. M. Autry, Z. Chen, and L. R. Jones. 2000. Reexamination of the role of the leucine/isoleucine zipper residues of phospholamban in inhibition of the Ca^{2+} pump of cardiac sarcoplasmic reticulum. *J. Biol. Chem.* 275:41487–41494.
4. Kovacs, R. J., M. T. Nelson, H. K. Simmerman, and L. R. Jones. 1988. Phospholamban forms Ca^{2+}-selective channels in lipid bilayers. *J. Biol. Chem.* 263:18364–18368.
5. Decrouy, A., M. Juteau, S. Proteau, J. Teijiera, and E. Rousseau. 1996. Biochemical regulation of sarcoplasmic reticulum Cl^{-} channel from human atrial myocytes: involvement of phospholamban. *J. Mol. Cell. Cardiol.* 28:767–780.
6. MacLennan, D. H., and E. G. Kranias. 2003. Phospholamban: a crucial regulator of cardiac contractility. *Nat. Rev. Mol. Cell Biol.* 4:566–577.
7. Metcalfe, E. E., J. Zamoon, D. D. Thomas, and G. Veglia. 2004. $^{1}H/^{15}N$ heteronuclear NMR spectroscopy shows four dynamic domains for phospholamaban reconstituted in dodecylphosphocholine micelles. *Biophys. J.* 87:1205–1214.
8. Toyoshima, C., M. Asahi, Y. Sugita, R. Khanna, T. Tsuda, et al. 2003. Modeling of the inhibitory interaction of phospholamban with the Ca^{2+} ATPase. *Proc. Natl. Acad. Sci. USA.* 100:467–472.
9. Morita, T., D. Hussain, M. Asahi, T. Tsuda, K. Kurzydlowski, et al. 2008. Interaction sites among phospholamban, sarcolipin, and the sarco(endo)plasmic reticulum Ca^{2+}-ATPase. *Biochem. Biophys. Res. Commun.* 369:188–194.
10. Houndonougbo, Y., K. Kuczera, and G. S. Jas. 2005. Structure and dynamics of phospholamban in solution and in membrane bilayer: computer simulations. *Biochemistry.* 44:1780–1792.
11. Paterlini, M. G., and D. D. Thomas. 2005. The α-helical propensity of the cytoplasmic domain of phospholamban: a molecular dynamics simulation of the effect of phosphorylation and mutation. *Biophys. J.* 88:3243–3251.
12. Sugita, Y., N. Miyashita, T. Yoda, M. Ikeguchi, and C. Toyoshima. 2006. Structural changes in the cytoplasmic domain of phospholamban by phosphorylation at Ser16: a molecular dynamics study. *Biochemistry.* 45:11752–11761.
13. Pantano, S., and E. Carafoli. 2007. The role of phosphorylation on the structure and dynamics of phospholamban: a model from molecular simulations. *Proteins.* 66:930–940.
14. Zamoon, J., A. M. and David D. Thomas, and G. Veglia. 2003. NMR solution structure and topological orientation of monomeric phospholamban in dodecylphosphocholine micelles. *Biophys. J.* 85:2589–2598.
15. Metcalfe, E., N. Traaseth, and G. Veglia. 2005. Serine 16 phosphorylation induces an order-to-disorder transition in monomeric phospholamban. *Biochemistry.* 44:4386–4396.
16. Adams, P. D., I. T. Arkin, D. M. Engelman, and A. T. Brunger. 1995. Computational searching and mutagenesis suggest a structure for the pentameric transmembrane domain of phospholamban. *Nat. Struct. Mol. Biol.* 2:154–162.
17. Sansom, M. S. P., G. R. Smith, O. S. Smart, and S. O. Smith. 1997. Channels formed by the transmembrane helix of phospholamban: a simulation study. *Biophys. Chem.* 69:269–281.
18. Oxenoid, K., and J. J. Chou. 2005. The structure of phospholamban pentamer reveals a channel-like architecture in membranes. *Proc. Natl. Acad. Sci. USA.* 102:10870–10875.
19. Robia, S. L., N. C. Flohr, and D. D. Thomas. 2005. Phospholamban pentamer quaternary conformation determined by in-gel fluorescence anisotropy. *Biochemistry.* 44:4302–4311.
20. Nesmelov, Y., C. Karim, L. Song, P. Fajer, and D. Thomas. 2007. Rotational dynamics of phospholamban determined by multifrequency electron paramagnetic resonance. *Biophys. J.* 93:2805–2812.

21. Traaseth, N. J., R. Verardi, K. D. Torgersen, C. B. Karim, D. D. Thomas, et al. 2007. Spectroscopic validation of the pentameric structure of phospholamban. *Proc. Natl. Acad. Sci. USA.* 104:14676–14681.

22. Phillips, J. C., R. Braun, W. Wang, J. Gumbart, E. Tajkhorshid, et al. 2005. Scalable molecular dynamics with NAMD. *J. Comput. Chem.* 26:1781–1802.

23. MacKerell, Jr., A., D. Bashford, M. Bellott, R. L. Dunbrack, Jr., J. Evanseck, et al. 1998. All-atom empirical potential for molecular modeling and dynamics studies of proteins. *J. Phys. Chem. B.* 102:3586–3616.

24. MacKerrel, A. D., M. Feig, and C. L. Brooks III. 2004. Extending the treatment of backbone energetics in protein force fields: limitations of gas-phase quantum mechanics in reproducing protein conformational distributions in molecular dynamics simulations. *J. Comput. Chem.* 25:1400–1415.

25. Allen, M. P., and D. J. Tildesley. 1987. Computer Simulation of Liquids. Oxford University Press, New York.

26. Martyna, G. J., D. J. Tobias, and M. L. Klein. 1994. Constant pressure molecular dynamics algorithms. *J. Chem. Phys.* 101:4177–4189.

27. Batcho, P. F., D. A. Case, and T. Schlick. 2001. Optimized particle-mesh Ewald/multiple-time step integration for molecular dynamics simulations. *J. Chem. Phys.* 115:4003–4018.

28. Jorgensen, W. L., J. Chandrasekhar, J. D. Madura, R. W. Impey, and M. L. Klein. 1983. Comparison of simple potential functions for simulating liquid water. *J. Chem. Phys.* 79:926–935.

29. Marrink, S. J., A. H. de Vries, and A. E. Mark. 2004. Coarse grained model for semiquantitative lipid simulations. *J. Phys. Chem. B.* 108: 750–760.

30. Marrink, S. J., and A. E. Mark. 2003. Molecular dynamics simulation of the formation, structure, and dynamics of small phospholipid vesicles. *J. Am. Chem. Soc.* 125:15233–15242.

31. Shih, A. Y., A. Arkhipov, P. L. Freddolino, and K. Schulten. 2006. Coarse grained protein-lipid model with application to lipoprotein particles. *J. Phys. Chem. B.* 110:3674–3684.

32. Marrink, S. J., H. J. Risselada, S. Yefimov, D. P. Tieleman, and A. H. de Vries. 2007. The MARTINI forcefield: coarse grained model for biomolecular simulations. *J. Phys. Chem. B.* 111:7812–7824.

33. Humphrey, W., A. Dalke, and K. Schulten. 1996. VMD: visual molecular dynamics. *J. Mol. Graph.* 14:33–38.

34. Lauterwein, J., C. Bosch, L. Brown, and K. Wuthrich. 1979. Physicochemical studies of the protein-lipid interactions in melittin-containing micelles. *Biochim. Biophys. Acta.* 556:244–264.

35. Anishkin, A., and S. Sukharev. 2004. Water dynamics and dewetting transitions in the small mechanosensitive channel MscS. *Biophys. J.* 86:2883–2895.

36. Gullingsrud, J., R. Braun, and K. Schulten. 1999. Reconstructing potentials of mean force through time series analysis of steered molecular dynamics simulations. *J. Comput. Phys.* 151:190–211.

37. Smart, O. S., J. G. Neduvelil, X. Wang, B. A. Wallace, and M. S. P. Sansom. 1996. HOLE: a program for the analysis of the pore dimensions of ion channel structural models. *J. Mol. Graph.* 14:354–360.

38. Gullingsrud, J., and K. Schulten. 2004. Lipid bilayer pressure profiles and mechanosensitive channel gating. *Biophys. J.* 86:3496–3509.

39. Liu, Y., and J. F. Nagle. 2004. Diffuse scattering provides material parameters and electron density profiles of biomembranes. *Phys. Rev. E Stat. Nonlin. Soft Matter Phys.* 69:040901.

40. Aksimentiev, A., and K. Schulten. 2005. Imaging α-hemolysin with molecular dynamics: ionic conductance, osmotic permeability and the electrostatic potential map. *Biophys. J.* 88:3745–3761.

41. Anishkin, A., B. Akitake, and S. Sukharev. 2008. Characterization of the resting MscS: modeling and analysis of the closed bacterial mechanosensitive channel of small conductance. *Biophys. J.* 94:1252–1266.

42. Isralewitz, B., S. Izrailev, and K. Schulten. 1997. Binding pathway of retinal to bacterio-opsin: a prediction by molecular dynamics simulations. *Biophys. J.* 73:2972–2979.

43. Kim, T., J. Lee, and W. Im. 2009. Molecular dynamics studies on structure and dynamics of phospholamban monomer and pentamer in membranes. *Proteins.* 76:86–88.

44. Park, S., and S. Opella. 2005. Tilt angle of a trans-membrane helix is determined by hydrophobic mismatch. *J. Mol. Biol.* 350:310–318.

45. Yeagle, P., M. Bennett, V. Lemaître, and A. Watts. 2007. Transmembrane helices of membrane proteins may flex to satisfy hydrophobic mismatch. *Biochimica et Biophysica Acta.* 1768:530–537.